2024 IEEE/RSJ International Conference on Intelligent Robots and Systems (IROS)
October 14-18, 2024. Abu Dhabi, UAE

Functional kinematic and kinetic requirements of the upper limb during activities of daily living: a recommendation on necessary joint capabilities for prosthetic arms

Christopher Herneth[1], Amartya Ganguly[1] and Sami Haddadin[1]

***Abstract*— Prosthetic limb abandonment remains an unsolved challenge as amputees consistently reject their devices. Current prosthetic designs often fail to balance human-like performance with acceptable device weight, highlighting the need for optimised designs tailored to modern tasks. This study aims to provide a comprehensive dataset of joint kinematics and kinetics essential for performing activities of daily living (ADL), thereby informing the design of more functional and user-friendly prosthetic devices. Functionally required Ranges of Motion (ROM), velocities, and torques for the Glenohumeral (rotation), elbow, Radioulnar, and wrist joints were computed using motion capture data from 12 subjects performing 24 ADLs. Our approach included the computation of joint torques for varying mass and inertia properties of the upper limb, while torques induced by the manipulation of experimental objects were considered by their interaction wrench with the subject's hand. Joint torques pertaining to individual ADL scaled linearly with limb and object mass and mass distribution, permitting their generalisation to not explicitly simulated limb and object dynamics with linear regressors (LRM), exhibiting coefficients of determination R = 0.99 $\pm$ 0.01. Exemplifying an application of data-driven prosthesis design, we optimise wrist axes orientations for two serial and two differential joint configurations. Optimised axes reduced peak power requirements, between 22% to 38% compared to anatomical configurations, by exploiting high torque correlations ($r = -0.84, p < 0.05$) between Ulnar deviation and wrist flexion/extension joints. This study offers critical insights into the functional requirements of upper limb prostheses, providing a valuable foundation for data-driven prosthetic design that addresses key user concerns and enhances device adoption.**

I. Introduction

Prosthetic limbs are crucial in improving lives and empowering individuals with limb amputations. However, despite extensive research, 23-50% of prosthetic users do not use their devices consistently [1], [2]. Prosthesis non-use and resulting unilateral performance may lead to cumulative trauma and severe injury of the remaining limb [3]–[5], accentuating the need for user-friendly prosthetics. At the same time, 72% of prosthesis non-users with limb differences would reconsider wearing a device if certain improvements were to be made [2].

Excessive device weight and poor weight distribution were identified as key concerns for users [2], [6], [7], ranking as the second most influential aspect for device abandonment after socket comfort [8]. Additional factors associated with high levels of dissatisfaction pertain to prosthesis agility, strength and control. Concurrently, upper limb prostheses were shown to be of limited effectiveness in basic tasks concerning independent living, work, household, and hobby [9], [10], while grabbing, picking up, and holding were considered essential prosthesis capabilities by users [9].

Achieving human-like performance within acceptable device weight is challenged by the limitations of current state-of-the-art actuator technologies. However, prosthetic technologies need not imitate human capabilities but rather be optimised for modern tasks, addressing user concerns. Optimisation and dimension of drive-train topology and components necessitate joint kinematics and kinetics during representative activities of daily living (ADL). Literature on functionally required Range of Motion (RoM) is abundant, with [11]–[15] covering an extensive range of tasks.

Explicit studies on ADL joint velocities are comparatively sparse, with [16], [17] focused on small task and joint sets and [18] on industrial environments (parts assembly). However, joint velocities can be estimated by differentiation of reported joint angle trajectories of RoM studies.

Functionally required joint kinetics are currently lacking in the literature. The authors are only aware of a singular study [19] and its derivative [20] reporting upper limb joint torques for various ADL tasks. Object manipulation is a cardinal aspect of ADL, often resulting in joint torques that surpass those related to limb movement. However, ADL joint torques induced by objects were not considered in [19], [20], while limb motion-related torques were only examined for limb mass and mass distribution pertaining to the healthy human limb. Consequently, the data reported in [19], [20] is of limited usefulness for optimising prosthetic devices exhibiting different dynamic properties. At the same time, neglecting manipulated objects might render resulting mechanisms incapable of completing particular ADL tasks.

Different methods have been proposed for the considera-

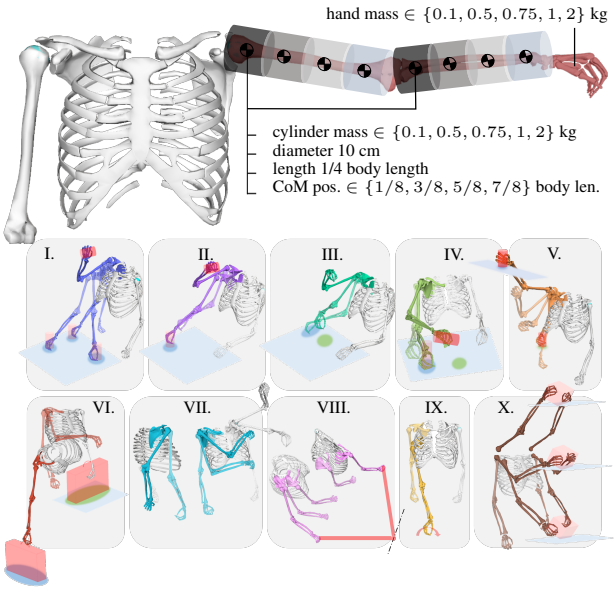

Fig. 1. Top: Composition of dynamic limb models. 20 cylinders (5 masses, 4 positions) on the humerus; 20 cylinders (5 masses, 4 positions) on the Ulna; 5 hand masses. Bottom: Experimental task set with illustrations outlining trial motion patterns during the manipulation phase and utilised experimental objects.

[1]Christopher Herneth, Amartya Ganguly, and Sami Haddadin are with Chair of Robotics and Systems Intelligence, MIRMI - Munich Institute of Robotics and Machine Intelligence, Technical University of Munich (TUM), Munich, Germany {christopher.herneth, amartya.ganguly, haddadin}@tum.de

tion of object dynamics in Inverse Dynamics (ID) simulations of ADL tasks. Muller et al. estimated L5/S1 moments during object transferring tasks by modelling loads as a point mass, whose kinematics were inferred from hand motions [21]. Akhavanfar et al. investigated differences in predicted spinal loads during bimanual lifting tasks [22]. External loads were simulated as unidirectional gravitational loads, additive object mass and inertia to the hand, and wrench-based methods, with experimental object motions tracked by motion capture. Wrench-based procedures were found to be more accurate, producing the least dynamic inconsistencies. Additionally, complex manipulation scenarios where objects are constrained by the environment (e.g., doors, keys, knobs) can be considered by their associated interaction wrench with the hand. Wrench-based methods require accurate object motions $\in \mathbb{R}^6$, which are seldomly reported in ADL datasets, with [23], [24] being notable exceptions. However, object kinematics can be accurately calculated from optical hand and wrist marker trajectories [25], commonly reported in ADL databases.

Quality data on task requirements enables data-driven optimisation of mechanism kinematic and dynamic parameters. In [26], the parallel kinematics of a 3 Degree of Freedom (DoF) parallel wrist were optimised for a specified task, effectively reducing required actuator torques. In [27], [28], authors optimised the transparency and topology of assistive devices based on the data reported in [19]. Damerla et al. [29] created a lightweight prosthetic wrist prototype based on functional requirements in joint RoM and velocity. At the same time, the lack of representative data necessitated the oversizing of joint torque capabilities to peak human strength.

In this study, we provide quantifiable parameters, such as joint RoM, velocities, and joint kinetics, necessary for ADL, that can inform prosthetic device design processes. Joint kinematics were extracted from [30], reporting optical marker trajectories of 12 subjects performing 24 ADL. Joint kinetics were computed for a stack of 45 unique limb models per trial, with object-induced torques simulated as described in [25]. Linear Regression Model (LRM)s trained to torque data of different ADL tasks, and varying limb mass distributions and object weight permit the computation of necessary peak torques pertaining to limbs and objects of custom dynamic properties. Finally, the data-driven design of a prosthetic wrist is exemplified by optimising joint axis orientations, leveraging a strong correlation between wrist deviation and flexion/extension joint torques.

II. Materials and Methods

A. Activities of daily living dataset

Joint kinematics and kinetics simulations were based on the ADL Human Arm Motion Dataset (ADL Dataset) captured by Gloumakov et al. [30]. The database reports trajectories of 55 optical markers recorded for 12 subjects (6 male, 6 female) completing 18 unimanual and 6 bimanual prescribed ADL (3 repetitions per task) deemed necessary for independent living. Individual trials distinguished three phases:

1) start in a defined pose followed by a reaching motion towards experimental objects
2) physical object manipulation according to experimental procedures outlined in [31]
3) returning motion to the starting posture

In this work, ADL Dataset trials were grouped into ten ADL tasks based on primitive motions pertaining to each trial's manipulation phase identified in [31], [32]. Task categories were: I. standing, and II. seated drinking from a cup/mug, III. eating with a fork/spoon, IV. pouring a liquid from a bottle, V. standing overhead picking a tin can, VI. lifting a briefcase from the ground to a tabletop, VII. hygiene (washing axilla and perineal), VIII. opening a door, IX. turning a key/door knob, and X. bimanual placement of a box between 3 shelf heights (low, medium, high). Individual task categories capture different aspects of daily living and the associated requirements for limb joints. The manipulation motions of individual task categories are illustrated in Fig. 1. In the following, limb joints are abbreviated with SR for Glenohumeral internal(+) / external(-) rotation, EF for elbow flexion(+) / extension(-), PS for forearm pronation(+) / supination(-), WF for wrist flexion(+) / extension(-), and WD for wrist Ulnar(+) / Radial(-) deviation.

B. Joint kinematics simulations

Joint kinematics were computed from optical marker trajectories and subject-specific simulation models with the OpenSim (version 4.4) Python API [33]. Upper body models were constructed based on the bimanual version of the MoBL-ARMS Dynamic Upper Limb Model (MoBL-ARMS DULM) [34]. Limits on the RoM of the wrist deviation axis were increased from 10° Radial, and 25° Ulna deviation to 25° and 50° respectively. Subject-specific models were generated from individual static trials by scaling the dimension of the MoBL-ARMS DULM with the OpenSim scaling tool. Anatomical - maximal and Root Mean Square (RMS) marker errors were 1.05 ± 0.2 cm and 0.66 ± 0.11 cm, respectively.

Inverse kinematics were computed with the OpenSim Inverse Kinematics (IK) solver, with joint velocities derived by second-order approximation from low-pass filtered (3rd order, 6 Hz) joint angle trajectories. Trials exhibiting outliers in joint velocities (peaks larger than 1.5 times the inter-quartile range) or maximal IK marker errors $>$ 10cm were discarded from our analysis (126 of 864 = 24 experiments * 12 subjects * 3 repetitions). Additionally, slowed joint trajectories were computed by local and proportional deceleration of all joints, such that peak joint velocities never exceeded the 99th percentile velocities of individual joint directions, computed across all full-speed trials. Resulting motions follow the same spatial limb trajectories as full-speed trials.

C. Joint kinetics simulations

Torques necessary for the production of low-pass filtered (3rd order, 6 Hz) joint motions (full-speed) of 738 (864-126) individual trials were simulated for:

1) varying mass and mass-distribution of the upper arm, forearm, and the hand
2) wrenches on the hand produced by the manipulation of objects in individual trials

ID simulations were carried out with the Python API of the OpenSim (version 4.4) ID tool.

1) Torques for limb motion: Joint torques were simulated for 45 MoBL-ARMS DULMs per subject, with unique dynamic properties of either Humerus, Ulna, or hand bodies. Initially, the mass and inertia of all bodies (except the thorax) were set to 0, while all muscles and passive forces were removed. Subsequently, individual models were constructed:

- Upper arm: modelled from individual cylinders of 10 cm diameter and a mass $\in M = \{0.1, 0.5, 0.75, 1, 2\}$ kg. Cylinder lengths were 1/4 of the subject's Humerus. The cylinder's Center of Mass (CoM) was positioned at intervals $\in \{1/8, 3/8, 5/8, 7/8\}$ of the subject's

Humeral length such that the cylinder's axis aligned with the Humerus' (refer to Fig. 1) - 20 models (5 masses at 4 positions).
- Forearm: modelled likewise to the upper arm, considering the subject's Ulnar lengths and axes - 20 models (5 masses at 4 positions).
- Radius: 0 mass and inertia.
- Hand: the subject models' hand mass and inertia properties were scaled to masses $\in M$ kg - 5 models (5 masses).

Trials exhibiting torque peaks larger than 3 times the median torque across all trials of an ADL (12 subjects, 3 repetitions) were excluded (69 of 738), resulting in 30105 ((736 - 69) trials * 45 models) valid ID simulations.

2) Torques induced by object manipulation: Optical markers and force measurements were absent for the objects reported in the ADL Dataset. Instead, trials were augmented with simulated objects. The interaction between the subject's hands and manipulated objects was modelled as the wrench necessary to move objects along prescribed trajectories. Object kinematics and interaction wrench $\in \mathbb{R}^6$ were estimated from wrist and hand markers with the ObjectAugmentationAlgorithm [25], grasping information available in [30]–[32], and task-specific object models described in table I. Joint torques pertaining to objects in bi-manual trials of task X were computed as outlined in [22]. Task IX (Key/Knob turning) was simulated by applying a static torque around the door knob or key axes to the hand. Tasks III (fork/spoon) and VII were not augmented. Object-related torque terms were isolated by setting all passive forces in the model and mass and inertia of Humerus, Ulna, Radius, and hand bodies to 0. The interaction wrench was applied to the hand by an external loads setup.

TABLE I
PARAMETERS OF VIRTUAL OBJECTS USED IN EACH TASK

Task	Object	Osim	Dimensions [mm]	Mass/Torque
I /II	Cup	Cylinder	r =43; h=100; handle=40	0.1, 0.5, 1 (kg),
	Mug	Cylinder	r =38.5; h=132; handle=30	0.1, 0.5, 1 (kg)
IV	Bottle	Cylinder	r=32; h=213	0.1, 0.5, 1, 1.5 (kg)
V	Tin Can	Cylinder	r=36.5; h=110	0.1, 0.5, 1 (kg)
VI	Briefcase	Box	x=450; y=350; z=110	1, 3, 5 (kg)
VIII	Door	Box	x=40; y=2032; z=890	9, 18, 33 (kg)
IX	Key			$\pm$ 0.3, 1.3, 2.3 (Nm)
	Knob			0,3, 1.3, 2.3 (Nm)
X	Box	Box	x=340; y=200; z=130	0.1, 1, 2, 5 (kg)

3) Limb and object torque regression: The results obtained in sections II-C.1, and II-C.2 are now generalized, by fitting LRMs to statistical torque quantities of individual joints. Resulting LRMs allow the computation of joint torques caused by mass distributions not explicitly simulated. Individual LRMs are fitted to joint torque percentiles $p \in \{0, 25, 50, 75, 100\}$ caused by the models of the upper arm, forearm, hand and object models described above. Each LRM's parameter $K_{p,C}$ was fitted to a specific p and a combination C of a joint $J \in \{$SR, EF, PS, WF, WD$\}$, a task $T \in \{$I, II, III, IV, V, VI, VII, VIII, IX, X$\}$, and a body $B \in \{$Humerus, Ulnar, Hand, Object$\}$ according to (1). For Humerus and Ulnar bodies, $\tau_{p,C}$ collected 20 torque values at the p_{th} percentile for each C, caused by the 20 cylinders described in section II-C.1. Their independent variable X_{cyl} was the vector of cylinder CoM position d [m] ($d <$ half the cylinder length is not permitted), and cylinder mass m [kg] products (1), with $K_{p,C}$ describing the slope of specific joint torque percentiles with cylinder mass and position. Cylinder positions were $\{1/8, 3/8, 5/8, 7/8\}$ multiplied by the average Humeral/Ulnar length over all subjects. For the hand $\tau_{p,C}$ collected 5 torque values at the p_{th} percentile for each C, caused by 5 different hand masses X_{hand}. Hand and cylinder masses were $\{0.1, 0.5, 0.75, 1, 2\}$ kg. Objects' $\tau_{p,C}$ collected torque percentile values for each C caused by the manipulation of the task-specific objects described in table I. Each object X_{obj} corresponded to its specific mass or static torque. The hand and objects $K_{p,C}$ describe the slope of percentile joint torques with increasing hand/object mass (or static torque). Torque percentiles p were computed over all trials (12 subjects, 3 repetitions) associated with a C. The items 'Cup' and 'Knob' were not considered in the regression analysis since task-specific object torques could not be described by linear models for varying object inertia and static torque signs.

$$\begin{aligned} \tau_{p,C} &= K_{p,C} X \\ X_{cyl} &= |m_1 * d_1, m_2 * d_2, ..., m_{20} * d_{20}| \\ X_{hand} &= |m_1, m_2, ...m_5| \\ X_{obj} &= |m_1, m_2, ..., m_n| \end{aligned} \tag{1}$$

The superposition principle allows the computation of a composite body's total joint torque requirements by summing the components' torque contributions. Consequently, joint torques for a limb constructed of several cylinders manipulating a specific object can be calculated by adding individual torque contributions. The latter may be computed with the help of the LRMs fitted above, allowing the prediction of ADL-specific 0th, and 100th percentile joint torques for composite, cylinder-based limb mass distributions and task-specific objects. Torques of individual components at the 25th, 50th, and 75th percentile cannot be summed to respective percentiles of the composite limb, since percentile computations need to consider individual data points. For SR, torque estimations must be calculated as the sum over relevant Humeral, Ulnar, and hand models. In EF, Ulnar and hand models must be considered, whereas only hand models are relevant for PS, WF, and WD. As an example, the maximal wrist flexion torque (p=100th, J=WF) during the uni-manual lifting task (T=VI), for a hand (B=Hand) weighing 0.5kg, and a briefcase weighing 1.25kg can be computed according to

$$\begin{aligned} \tau_{100th, C_{Hand}\{WF,VI,Hand\}, C_{Brief.}\{WF,VI,Brief.\}} = \\ K_{100th, C_{Hand}} * 0.5 + K_{100th, C_{Brief.}} * 1.25 \end{aligned}$$

D. Wrist axes optimization

This section exemplifies a data-informed design approach for prosthesis joint and actuator design in the example of the wrist. An optimal orientation $\theta \in \{\theta_A, \theta_B\}$ of wrist actuation axes was computed by minimising the maximal sum of simultaneously occurring, absolute actuator powers P in rotated axes (2). Axis index A relates to the WF axis rotated by θ_A, with index B describing the rotated WD axis (θ_B) (2).

$$\min_{\theta} \quad \max(|P_A(\theta_A)|) + \max(|P_B(\theta_B)|) \tag{2}$$

P was calculated across all trial's joint velocity and torque pairs, computed in sections II-B, and II-C.1, for a hand weighing 0.5kg. Object induced torques are neglected in this example. Input velocities were capped at WF velocities -300 °/s $< \nu_{WF} <$ 300 °/s and WD velocities at -102 °/s $< \nu_{WD} <$ 102 °/s, corresponding to $\pm$ 99th percentile joint velocities, deemed sufficient for ADL. The matrices τ and

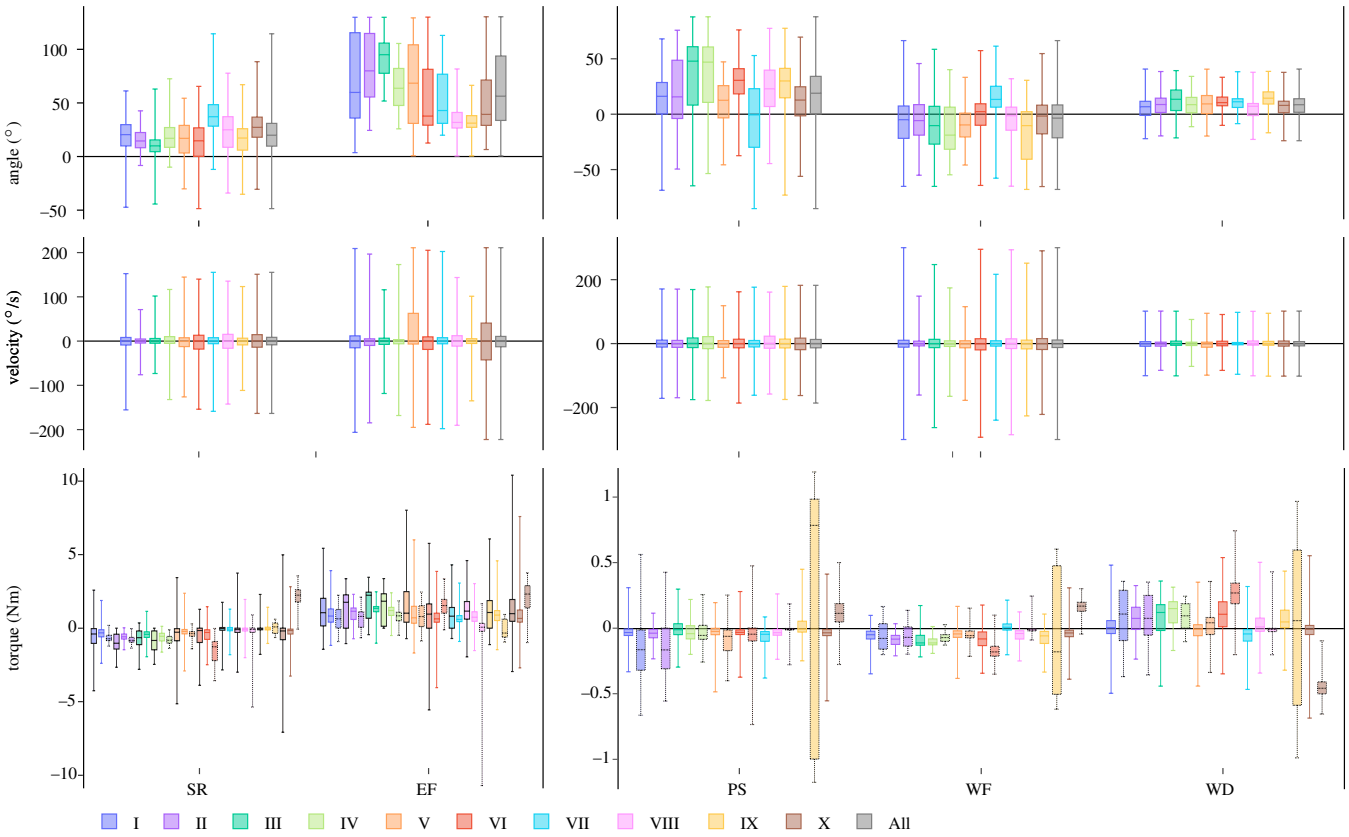

Fig. 2. Box plots for joint angles (°) (row 1), joint velocities (°/s) (row 2), and joint torques (Nm) (row 3). Boxes are specific to joints and tasks, with data concatenated over all subjects and repetitions. Torque Box plots were computed for the Ulna - solid black outline (4 cylinders as depicted in Fig. 1 of 0.5kg each), the hand - coloured outline (0.5 kg) and selected task objects $\in \{I$ (Mug 0.5 kg), II (Mug 0.5 kg), IV (Bottle 0.5 kg), V (Briefcase 1kg), VI (Tin can 0.5kg), IX (Key 1.3Nm), X (Box 1kg)$\}$ - dashed black outline.

ν contain paired torque and velocity trajectories of WF and WD joints concatenated over all trials.

Wrist joint axes were optimized for four cases:

- **Serial actuation with orthogonal joint axes.** The actuator power for each new axes was calculated by (3) with axes A and B orthogonal but rotated by $\theta = \theta_A = \theta_B$ from the anatomic orientation.
$$P = R(\theta)(\tau \odot \nu) \tag{3}$$
$\odot$ denotes the Hadamard product.
- **Serial actuation with non-orthogonal joint axes.** Axes A and B were rotated by distinct angles θ_A and θ_B. Actuator powers in the rotated system evaluate to (4), with K^{-1} describing the individual rotation of both axes.
$$P = K^{-1}(\tau \odot \nu) \tag{4}$$
$$K = \begin{Bmatrix} \cos(\theta_A) & \cos(\theta_B) \\ \sin(\theta_A) & \sin(\theta_B) \end{Bmatrix}^{-1} \tag{5}$$
- **Differential actuation with orthogonal joint axes.** The wrist joint is formed by a differential drive consisting of two actuators and two orthogonal joint axes, rotated by $\theta = \theta_A = \theta_B$ from the anatomic orientation. Joint torques and velocities were calculated from actuator torques and velocities to (7) and (8), respectively [35]. Actuator powers for the rotated mechanism were calculated with (6).
$$P = (T_\tau^{-1} R(\theta)\tau) \odot (T_\nu^{-1} R(\theta)\nu) \tag{6}$$
$$T_\tau^{-1} = \begin{Bmatrix} 1 & 1 \\ 1 & -1 \end{Bmatrix}^{-1} \tag{7}$$
$$T_\nu^{-1} = \begin{Bmatrix} 0.5 & 0.5 \\ 0.5 & -0.5 \end{Bmatrix}^{-1} \tag{8}$$
- **Differential actuation with non-orthogonal joint axes.** The wrist joint is formed by a differential drive consisting of two actuators and two non-orthogonal joint axes. Joint axes are rotated by distinct angles θ_A and θ_B from the anatomic orientation. Consistent with DO, joint torques and velocities were calculated to (7) and (8). Similarly, actuator powers for the rotated mechanism (9) were calculated by replacing the rotation matrix R in (6) with the coefficient matrix K (5), introduced in the SNO configuration.
$$P = (T_\tau^{-1} K^{-1} \tau) \odot (T_\nu^{-1} K^{-1} \nu) \tag{9}$$

III. Results

This section presents functional joint kinematics and kinetics of human subjects engaging in various ADL. Results of IK simulations pertain to joint angle, velocity and marker error trajectories. ID outcomes treat joint torque profiles produced by varying limb mass distributions and torques induced by object manipulation. Sections II-B, and II-C.1 inform about exclusion criteria of individual trials from subsequent analysis.

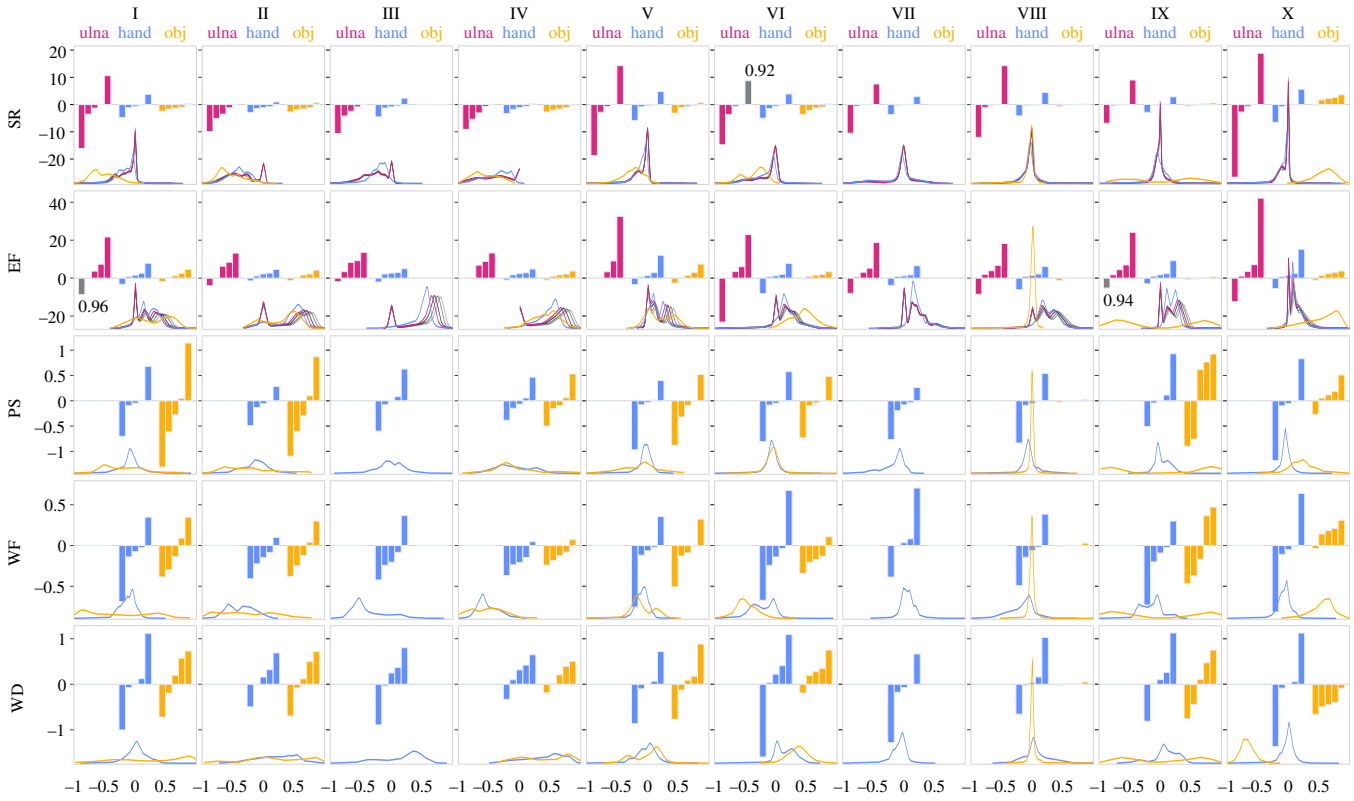

Fig. 3. Coefficients of linear regression models fitted to percentile joint torques. Colours distinguish forearm (red), hand (blue), and object (yellow) dynamics models. The magnitude of each K_C is indicated by the bar height with percentile models ($p \in \{0, 25, 50, 75, 100\}$) ordered left to right. Grey bars mark models with coefficients of determination R < 0.99. Density plots indicate the torque distributions of normalized joint torques, used in the model fitting. Red: torques produced by a cylinder placed at the most proximal Ulna position (1/8). Grey-scale: positions (3/8, 5/8, 7/8). Blue: torques produced by the hand. Yellow: object induced torques.

A. ADL joint kinematics

1) Inverse kinematics errors: Table II reports maximal and RMS errors occurring in IK simulations of individual task-types. Maximal errors were the maximally occuring L2 distance (cm) between optical markers of the input dataset and associated virtual markers placed on the MoBL-ARMS DULM across all frames of trials related to a task. RMS errors were computed accordingly as the average across all trials of a task of maximum RMS errors between markers within individual trials. Maximal errors were 6.88 $\pm$ 1.23 cm and RMS errors were 0.15 $\pm$ 0.02 cm.

TABLE II
TASK SPECIFIC MARKER ERRORS.

Error	I	II	III	IV	V	VI	VII	VIII	IX	X
Max	7.41	6.71	5.67	5.20	8.08	5.76	7.38	6.25	6.82	9.55
RMS	0.15	0.17	0.17	0.17	0.11	0.13	0.17	0.11	0.14	0.17

2) Joint angles: Fig. 2 reports box-plots of ADL-task specific joint angles, calculated from angle trajectories of each subject's dominant limb.

- Functional SR spanned from 114° of internal rotation for hygiene tasks (VII) to 49° of external rotation for standing pick and drink (I), eating (III), and uni-manual lifting (VI) tasks.
- Elbow excursions reached 130° for tasks I-III, overhead picking (V), VI, and bi-manual pick and place (X). Full elbow extension was observed for tasks I, V, opening a door (VIII), and door key/knob turning (IX).
- Forearm pronation angles were maximal for seated eating and pouring tasks (III, IV) 88°, while supination angles reached 86° during the hygiene task.
- Wrist flexion peaked around 66° for tasks I, III, VI, VII, and X, whereas extension was similar across tasks at 68°, except for V.
- Wrist deviation requirements were consistent across all task types, except IV, VI, and VIII, with 41° of Ulnar and 24° of Radial deviation.

3) Joint velocities: Fig. 2 (second row) shows joint velocity box-plots of individual joints and tasks computed for the slowed motion trajectories described in section II-B.

- SR velocities were confined by tasks I, V, VI, VII, and X, ranging from 155 °/s internal to 164 °/s external rotation.
- EF velocities were maximal for the same tasks as in SR with the addition of task II, reaching 211 °/s in flexion and 222 °/s in extension.
- PS velocities peaked around 182 °/s pronation and 186 °/s supination for all tasks except V.
- WF velocities were highest in tasks I, VI, VIII, and X at 300 °/s flexion and 300 °/s extension. As in PS, task V exhibited the lowest speed.
- WD velocities were uniform across tasks, at 102 °/s in ulnar deviation and 102 °/s in radial deviation.

B. ADL joint kinetics

Fig. 2 (third row) depicts box plots of individual joint torque contributions of the forearm, hand, and selected objects. Maximal and minimal quantities can be scaled to individual requirements with fitted LRMs. Additionally, quartile and median values can be scaled for hand and object models since they do not require model superposition for individual contributions (see section II-C.3). Fig. 3 collects

TABLE III

WRIST RANGE OF MOTION, TORQUE, VELOCITY AND POWER REQUIREMENTS FOR OPTIMIZED WRIST CONFIGURATIONS.

Axis	Axis angle [°]	RoM [°, %]		τ [Nm, %]		ν [°/s, %]		P [W, %]	
WD	0	44		0.8		273		2.3	
WF	90	69		0.4		209		1.3	
SO A	0	44	0	0.8	0	273	0	2.3	0
SO B	90	69	0	0.4	0	209	0	1.3	0
SNO A	23	58	33	0.8	8	302	10	1.6	-29
SNO B	109	66	-5	0.3	-21	300	44	0.8	-35
DO A	64	82	88	0.6	-23	426	56	1.6	-29
DO B	154	93	35	0.2	-44	407	95	0.9	-34
DNO A	60	76	74	0.5	-29	396	45	1.4	-38
DNO B	159	101	47	0.2	-40	443	112	1.0	-22

$K_{p,C}$ (height of coloured bars) of individual LRMs fitted to combinations of joints (rows), tasks (columns), and dynamic models (colours) at torque percentiles $\in \{0, 25, 50, 75, 100\}$ (bars left to right). Only 3/600 models exhibited coefficients of determination $R < 0.99$. Torque contributions of the upper arm were negligible relative to those of the forearm, hand, and objects and were therefore excluded from our analysis. Distributions below bars show the density of normalised joint torques used in the computation of depicted $K_{p,C}$ parameters (models fitted to non-normalized data). Numeric $K_{p,C}$ values can be found in the supplementary material.

- SR torques were in external rotation for all but 100th percentile torques, except for object torques in X. Lower percentiles showed greater sensitivity to Ulnar mass and inertia.
- EF torques were primarily positive (flexion), exhibiting an increased sensitivity to forearm mass and mass distribution.
- PS, WF, and WD torque percentiles were similarly influenced by hand and object mass in all tasks involving unconstrained objects (I-VI). Task VIII exhibited the least sensitivity to object mass, while Task IX maximised object-related peak and quartile torque requirements in all wrist and forearm joints. Similarly, increased quartile object torques were exhibited by task X.

C. Wrist optimisation

Table III summarises optimised axis orientations and their required RoM, torque (τ), velocity (ν), and power (W), as well as percentage changes to the anatomical baseline. Figure 4 shows torque samples (purple markers) across all trials in the wrist configuration plane, produced by a hand of 0.5kg mass. WF and WD torques exhibited a Pearson correlation coefficient -86 ($p < 0.05$). The principal components of WF and WD torques are depicted as black/grey lines, with the first principal component explaining 95% of total variance. Optimised A and B axes are displayed as coloured lines, with axis lengths corresponding to the required actuator powers.

In serial actuation with orthogonal joint axes (SO - blue), optimal wrist axes A and B aligned with anatomical WF and WD axes. Serial actuation with non-orthogonal joint axes (SNO - red) resulted in rotated WD and WF axes, coinciding with the first and second torque principal components. Optimisation for differential actuation with orthogonal joint axes (DO - green) and differential actuation with non-orthogonal joint axes (DNO - purple) produced similar A and B axes, wedged centrally between principal components. Optimised joint axes resulted in power reductions from 22% to 38%, compared to the baseline. However, joint requirements of optimised axes were susceptible to specific axes orientations, as demonstrated by the varying actuator requirements for nearly overlapping joint axes in DO and DNO.

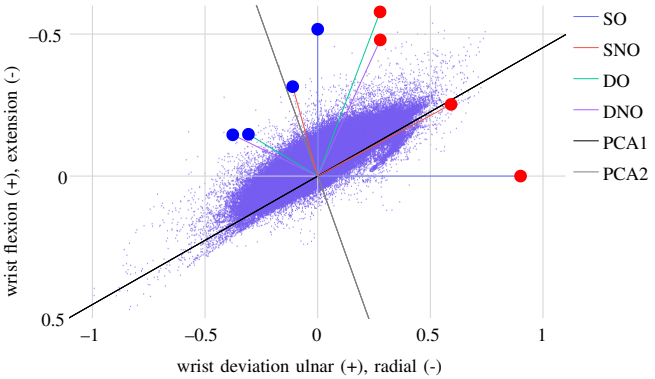

Fig. 4. Optimized wrist joint axes and torque principal components in the wrist configuration space. Axes lengths correspond to the required actuator power, with blue and red markers indicating axes A and B, respectively. Purple markers indicate torque samples normalised by $max\sqrt{\tau_{WF}^2 + \tau_{WD}^2}$.

IV. DISCUSSION

This study simulated joint kinematics and kinetics of 18 unimanual and 6 bimanual ADL based on optical marker trajectories of 12 subjects reported in the ADL Dataset. [30]. The OpenSim Api (4.4) [33] was employed for IK and ID computations, with subject-specific models derived by static scaling of the MoBL-ARMS DULM. RoM constraints of the model's wrist deviation axes were increased since previous research [11], [12], [36], [37] showed maximal ADL joint excursion above the set joint limits.

Table IV collects our recommendations on functionally necessary joint RoM, derived as maximally observed joint excursions during the considered ADL. Fig. 5 compares our results with functional joint RoM described in the literature. Shoulder internal and external rotation (SR), elbow flexion (EF), forearm supination, and wrist deviation (WD) were within $\pm$ 1 SD of previously reported ADL joint excursions. Pronation and wrist flexion/extension requirements were found to be more prominent in this study. The absence of additional hygiene tasks, like combing one's hair, caused comparatively low functional internal rotation angles. Consequently, we increased our recommendation for necessary prosthesis internal SR RoM from 49° to 90° (IV, bracketed value), based on the results detailed in [38]–[40]. The variations in functionally necessary RoM reported between studies underline the importance of selecting representative ADL tasks for analysis. Concurrently, unilateral amputees perform unimanual tasks primarily with the intact limb [3]–[5], [41]. This includes tasks requiring fine motor control and sensitive tasks such as tooth brushing and combing. On the other hand, bi-manual tasks, such as feeding, require

TABLE IV

ADL-BASED, FUNCTIONAL PROSTHESIS RECOMMENDATIONS FOR JOINT ROM AND VELOCITIES.

	SR		EF		PS		WF		WD	
	int.	ext.	flex.	ext	pro.	sup.	flex.	ext.	Uln.	Rad.
RoM (°)	114	49 (90)	130	0	88	86	66	68	41	24
vel 99th (°/s)	155	164	211	222	182	186	300	300	102	102
vel max (°/s)	267	298	486	381	716	684	425	579	240	260

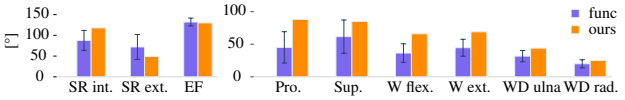

Fig. 5. Comparison functional joint RoM in this and previous studies

two capable limbs. Therefore, the definition of functional requirements of upper limb prosthetic devices needs to be carefully chosen based on intended usage scenarios (Tasks).

Joint motions inferred from captured marker trajectories via registration with virtual markers placed on subject models were shown to vary considerably, with small variations in virtual marker placement [42]. Consequently, joint kinematics and kinetics computed in this study represent one solution out of a set of equally probable trajectories pertaining to the particular placement of virtual markers on scaled subject models. Additionally, experiments with kinematic inconsistencies, such as gimbal-lock of the ground to thorax joint, associated with extreme velocity spikes, and trials with maximal marker errors above 10cm were excluded from our analysis. However, uncertainties in IK reconstructions may persist in reported data.

Joint velocities were calculated by second-order approximation from low-pass filtered joint angle trajectories. Filter cut-off frequencies were chosen to 6 Hz, following the standard settings of OpenSim. Table IV reports maximal and 99th percentile velocities of individual joint directions computed across all trials. 99th percentile speeds were substantially exceeded by peak velocities, observed in isolated trials of particular subjects. Therefore, prosthesis design based on maximal joint velocities is not recommended since it would lead to oversized drive trains. In contrast, industrial state-of-the-art prosthesis interfacing schemes do not permit concurrent control of high joint speeds [41]. Consequently, slow-motion trials were computed, allowing a more realistic view of functionally required joint speeds. Spatial limb trajectories in slow trials remained unchanged. At the same time, instantaneous joint velocities were simultaneously and proportionally decelerated such that maximal velocities did not exceed the 99th percentile velocities of respective full-speed joint velocities. Slowed trials exhibited 5 ± 6 % longer experiment durations, while required peak velocities were decreased by 53 ± 14 %, compared to full-speed trials. Consequently, actuators designed for functional joint speeds of marginally decelerated trials can be dimensioned for half the required peak actuator power. Complementary literature on ADL joint velocities is scarce, with [16] focused on a limited task set. Functional velocities described for internal (+15%) and external (+9%) shoulder rotation, elbow flexion (+28%), wrist extension (-3%) and Ulnar wrist deviation (+30%) compare well with our results. Percentage differences are compared to our recommendations based on 99th percentile velocities. Forearm Pronation was found to be 60% higher in [16], while the remaining joints were not reported.

The authors know only one relevant study, [19], and its derivative [43], discussing joint torques produced during a comprehensive set of ADL. Torques were computed via ID for limbs pertaining to healthy human subjects' mass and mass distribution. However, the design of prosthetic devices requires torques produced by the prosthetic mechanisms' specific dynamic properties. Instead, this study simulated joint torques for 45 unique dynamic models per subject and trial. Upper and forearm models consisted of cylinder segments of different masses and CoM locations, while the hand was modelled with 5 different weights. Additional to torques necessary for limb motion, interaction forces and moments caused by manipulating objects form a cardinal aspect of ADL, often resulting in joint torques that surpass those related to limb movement. However, objects were not considered in [19], [20], while [44] did not record motions pertaining to individual experimental items. We considered torques induced by object manipulation by applying the wrench necessary for prescribed object motion to the hand. Wrench-based methods were shown to reduce dynamic inconsistencies during ID [21], [22]. Required object motions $\in \mathbb{R}^6$ were estimated from optical marker trajectories of hand and wrist markers, using our ObjectAugmentationAlgorithm [25].

600 LRMs were fitted to percentile $p \in \{0, 25, 50, 75, 100\}$ joint torques produced by individual combinations of upper, forearm, hand, and object models, and different ADL tasks. Individual LRMs exhibited excellent coefficients of determination R = 0.99 $\pm$ 0.01, with only 3/600 models not demonstrating linear relationships between joint torques and limb dynamics. Linearity with cylinder CoM position was caused by the dominant influence of gravitational torques, which scale linearly with mass and CoM moment arms. Effects proportional to second moments were minor due to generally low ADL joint velocities and accelerations. ADL torque LRMs permit the prediction of joint toques pertaining to (cylinder-based) mass distributions not explicitly simulated. Superimposing the results of individual LRMs allows the designer of mechanisms resembling a human limb, the estimation of peak torques resulting from ADL limb motion and object manipulation. However, designers need to consider that limb mass, and available control schemes might lead to ADL joint trajectories distinct from the motions performed by healthy subjects utilised in this study.

ADL wrist torques caused by a hand weighing 0.5 kg (without objects) were aligned along an oblique axis, with the first principal component of WF and WD torques explaining 95% of total variance. This motivated optimising wrist axes orientations for 2 serial (SO, SNO) and 2 differential joint (DO, DNO) configurations, exemplifying data-driven design for upper-limb prosthetics and concomitant reductions in actuator requirements. The optimisation of serial and orthogonal axes produced a wrist configuration coincidental with anatomic joint definitions. Allowing axes to be non-orthogonal aligned individual axes with torque principal components. Optimised DO and DNO axes produced similar configurations, placing torque principal components between optimised axes such that their combined effort could be expanded for peak power requirements. Overall, power requirements of optimised axes orientations distinct from the anatomical configurations lead to reductions in peak power requirements of 22% to 38%. The optimisation of an entire prosthetic limb will be addressed in future works.

Our data provides a valuable basis for informed prosthesis development, keeping in mind the end-user and prevailing over technological limitations when addressing critical flaws in prosthetic device mass and dexterity.

V. Supplementary Material

Parameters $K_{p,C}$ and coefficients of determination R of individual LRMs may be found here: `https://github.com/ChristopherHerneth/Supplementary-Material-Publications`.
Additional video material may be accesses here: `https://youtu.be/WffbXRzqWqM`.

ACKNOWLEDGMENT

This work was supported by the Federal Ministry of Education and Research of the Federal Republic of Germany (BMBF) by funding the project AI.D under the Project Number 16ME0539K.

REFERENCES

[1] Monica Espinosa and Dan Nathan-Roberts. Understanding prosthetic abandonment. *Proceedings of the Human Factors and Ergonomics Society Annual Meeting*, 63(1):1644–1648, nov 2019.

[2] Elaine A. Biddiss and Tom T. Chau. Upper limb prosthesis use and abandonment. *Prosthetics and Orthotics International*, 31(3):236–257, sep 2007.

[3] Christina Rock Gambrell. Overuse Syndrome and the Unilateral Upper Limb Amputee: Consequences and Prevention. *JPO Journal of Prosthetics and Orthotics*, 20(3):126–132, July 2008.

[4] Kristin Østlie, Rosemary J. Franklin, Ola H. Skjeldal, Anders Skrondal, and Per Magnus. Musculoskeletal Pain and Overuse Syndromes in Adult Acquired Major Upper-Limb Amputees. *Archives of Physical Medicine and Rehabilitation*, 92(12):1967–1973.e1, December 2011.

[5] Linda Resnik, Marissa R. Meucci, Shana Lieberman-Klinger, Christopher Fantini, Debra L. Kelty, Roxanne Disla, and Nicole Sasson. Advanced Upper Limb Prosthetic Devices: Implications for Upper Limb Prosthetic Rehabilitation. *Archives of Physical Medicine and Rehabilitation*, 93(4):710–717, April 2012.

[6] Judith Davidson. A survey of the satisfaction of upper limb amputees with their prostheses, their lifestyles, and their abilities. *Journal of Hand Therapy*, 15(1):62–70, jan 2002.

[7] Francesca Cordella, Anna Lisa Ciancio, Rinaldo Sacchetti, Angelo Davalli, Andrea Giovanni Cutti, Eugenio Guglielmelli, and Loredana Zollo. Literature review on needs of upper limb prosthesis users. *Frontiers in Neuroscience*, 10, may 2016.

[8] Aimee E. Schultz, Susan P. Baade, and Todd A. Kuiken. Expert opinions on success factors for upper-limb prostheses. *The Journal of Rehabilitation Research and Development*, 44(4):483, 2007.

[9] Nienke Kerver, Corry K. van der Sluis, Sacha van Twillert, and Paul F. M. Krabbe. Towards assessing the preferred usage features of upper limb prostheses: most important items regarding prosthesis use in people with major unilateral upper limb absence—a dutch national survey. *Disability and Rehabilitation*, 44(24):7554–7565, November 2021.

[10] Elaine Biddiss, Dorcas Beaton, and Tom Chau. Consumer design priorities for upper limb prosthetics. *Disability and Rehabilitation: Assistive Technology*, 2(6):346–357, January 2007.

[11] Jaiyoung Ryu, William P. Cooney, Linda J. Askew, Kai-Nan An, and Edmund Y.S. Chao. Functional ranges of motion of the wrist joint. *The Journal of Hand Surgery*, 16(3):409–419, may 1991.

[12] David L. Nelson, Margaret A. Mitchell, Paul G. Groszewski, Stephen L. Pennick, and Paul R. Manske. Wrist range of motion in activities of daily living. In *Advances in the Biomechanics of the Hand and Wrist*, pages 329–334. Springer US, 1994.

[13] Mert Doğan, Mertcan Koçak, Özge Onursal Kılınç, Fatma Ayvat, Gülşah Sütçü, Ender Ayvat, Muhammed Kılınç, Özgür Ünver, and Sibel Aksu Yıldırım. Functional range of motion in the upper extremity and trunk joints: Nine functional everyday tasks with inertial sensors. *Gait and Posture*, 70:141–147, may 2019.

[14] Maheen Nadeem, Jeremy G. Loss, Zong-Ming Li, and William H. Seitz. Ulnar extension coupling in functional wrist kinematics during hand activities of daily living. *The Journal of Hand Surgery*, 47(2):187.e1–187.e13, feb 2022.

[15] Matthew Sardelli, Robert Z. Tashjian, and Bruce A. MacWilliams. Functional elbow range of motion for contemporary tasks. *Journal of Bone and Joint Surgery*, 93(5):471–477, mar 2011.

[16] Aïda M. Valevicius, Quinn A. Boser, Ewen B. Lavoie, Craig S. Chapman, Patrick M. Pilarski, Jacqueline S. Hebert, and Albert H. Vette. Characterization of normative angular joint kinematics during two functional upper limb tasks. *Gait and Posture*, 69:176–186, mar 2019.

[17] Gert-Åke Hansson, Istvan Balogh, Kerstina Ohlsson, Lothy Granqvist, Catarina Nordander, Inger Arvidsson, Ingrid Åkesson, Jeannette Unge, Ralf Rittner, Ulf Strömberg, and Staffan Skerfving. Physical workload in various types of work: Part i. wrist and forearm. *International Journal of Industrial Ergonomics*, 39(1):221–233, jan 2009.

[18] WILLIAM S. MARRAS and RICHARD W. SCHOENMARXLIN. Wrist motions in industry. *Ergonomics*, 36(4):341–351, apr 1993.

[19] J. Rosen, J.C. Perry, N. Manning, S. Burns, and B. Hannaford. The human arm kinematics and dynamics during daily activities - toward a 7 dof upper limb powered exoskeleton. In *ICAR '05. Proceedings., 12th International Conference on Advanced Robotics, 2005.* IEEE, 2005.

[20] Joel C. Perry, Janet M. Powell, and Jacob Rosen. Isotropy of an upper limb exoskeleton and the kinematics and dynamics of the human arm. *Applied Bionics and Biomechanics*, 6(2):175–191, jul 2009.

[21] Antoine Muller, Hakim Mecheri, Philippe Corbeil, André Plamondon, and Xavier Robert-Lachaine. Inertial motion capture-based estimation of l5/s1 moments during manual materials handling. *Sensors*, 22(17):6454, August 2022.

[22] Mohammadhossein Akhavanfar, Thomas K. Uchida, Allison L. Clouthier, and Ryan B. Graham. Sharing the load: modeling loads in OpenSim to simulate two-handed lifting. *Multibody System Dynamics*, 54(2):213–234, jan 2022.

[23] Franziska Krebs, Andre Meixner, Isabel Patzer, and Tamim Asfour. The kit bimanual manipulation dataset. *IEEE/RAS International Conference on Humanoid Robots (Humanoids)*, 2021.

[24] Christian Mandery, Oemer Terlemez, Martin Do, Nikolaus Vahrenkamp, and Tamim Asfour. The kit whole-body human motion database. *International Conference on Advanced Robotics (ICAR)*, 2015.

[25] Christopher Herneth, Junnan Li, Muhammad Hilman Fatoni, Amartya Ganguly, and Sami Haddadin. Object Augmentation Algorithm: Computing virtual object motion and object induced interaction wrench from optical markers, 2024.

[26] Soheil Zarkandi. Task-based torque minimization of a 3-prr spherical parallel manipulator. *Robotica*, 40(3):475–504, June 2021.

[27] Michael Fennel, Antonio Zea, and Uwe D. Hanebeck. Optimization-driven design of a kinesthetic haptic interface with human-like capabilities. *IEEE Transactions on Haptics*, 15(1):45–50, January 2022.

[28] Liansen Sha, Andi Lin, Qiang Xi, and Shaolong Kuang. A topology optimization method for robot light-weight design under multi-working conditions and its application on upper-limb powered exoskeleton. In *2020 International Conference on Artificial Intelligence and Electromechanical Automation (AIEA)*. IEEE, June 2020.

[29] Revanth Damerla, Kevin Rice, Daniel Rubio-Ejchel, Maurice Miro, Enrico Braucher, Juliet Foote, Issam Bourai, Aaryan Singhal, Kang Yang, Hongju Guang, Vasil Iakimovitch, Evelyn Sorgenfrei, and Shorya Awtar. Design and testing of a novel, high-performance two DoF prosthetic wrist. *IEEE Transactions on Medical Robotics and Bionics*, 4(2):502–519, may 2022.

[30] Yuri Gloumakov, Adam Spiers, and Aaron Dollar. Adl human arm motion data. IEEE Dataport: 10.21227/ayhf-q263, 2021.

[31] Yuri Gloumakov, Adam J. Spiers, and Aaron M. Dollar. Dimensionality reduction and motion clustering during activities of daily living: Three-, four-, and seven-degree-of-freedom arm movements. *IEEE Transactions on Neural Systems and Rehabilitation Engineering*, 28(12):2826–2836, dec 2020.

[32] Yuri Gloumakov, Adam J. Spiers, and Aaron M. Dollar. Dimensionality reduction and motion clustering during activities of daily living: Decoupling hand location and orientation. *IEEE Transactions on Neural Systems and Rehabilitation Engineering*, 28(12):2955–2965, dec 2020.

[33] Ajay Seth, Jennifer L. Hicks, Thomas K. Uchida, Ayman Habib, Christopher L. Dembia, James J. Dunne, Carmichael F. Ong, Matthew S. DeMers, Apoorva Rajagopal, Matthew Millard, Samuel R. Hamner, Edith M. Arnold, Jennifer R. Yong, Shrinidhi K. Lakshmikanth, Michael A. Sherman, Joy P. Ku, and Scott L. Delp. Opensim: Simulating musculoskeletal dynamics and neuromuscular control to study human and animal movement. *PLOS Computational Biology*, 14(7):e1006223, July 2018.

[34] Daniel C. McFarland, Emily M. McCain, Michael N. Poppo, and Katherine R. Saul. Spatial dependency of glenohumeral joint stability during dynamic unimanual and bimanual pushing and pulling. *Journal of Biomechanical Engineering*, 141(5), mar 2019.

[35] Keke Wang, Huihuan Qian, Yong Yang, and Yangsheng Xu. A novel differential modular robot joint and design and implementation. In *2013 IEEE International Conference on Robotics and Biomimetics (ROBIO)*. IEEE, dec 2013.

[36] Deanna H. Gates, Lisa Smurr Walters, Jeffrey Cowley, Jason M. Wilken, and Linda Resnik. Range of motion requirements for upper-limb activities of daily living. *The American Journal of Occupational Therapy*, 70(1):7001350010p1–7001350010p10, dec 2015.

[37] G. Brigstocke, A. Hearnden, C.A. Holt, and G. Whatling. The functional range of movement of the human wrist. *Journal of Hand Surgery (European Volume)*, 38(5):554–556, aug 2012.

[38] Carolien J. van Andel, Nienke Wolterbeek, Caroline A.M. Doorenbosch, DirkJan (H.E.J.) Veeger, and Jaap Harlaar. Complete 3d kinematics of upper extremity functional tasks. *Gait and Posture*, 27(1):120–127, jan 2008.

[39] D.J. Magermans, E.K.J. Chadwick, H.E.J. Veeger, and F.C.T. van der Helm. Requirements for upper extremity motions during activities of daily living. *Clinical Biomechanics*, 20(6):591–599, jul 2005.

[40] P. Raiss, O. Rettig, S. Wolf, M. Loew, and P. Kasten. Das bewegungsausmaß der schulter und des ellenbogens bei alltagsbewegungen in der 3d-bewegungsanalyse. *Zeitschrift für Orthopädie und Unfallchirurgie*, 145(04):493–498, oct 2007.

[41] Alix Chadwell, Laurence Kenney, Sibylle Thies, Adam Galpin, and John Head. The Reality of Myoelectric Prostheses: Understanding What Makes These Devices Difficult for Some Users to Control. *Frontiers in Neurorobotics*, 10, August 2016.

[42] Thomas K. Uchida and Ajay Seth. Conclusion or illusion: Quantifying uncertainty in inverse analyses from marker-based motion capture due to errors in marker registration and model scaling. *Frontiers in Bioengineering and Biotechnology*, 10, May 2022.

[43] Joel C. Perry, Janet M. Powell, and Jacob Rosen. Isotropy of an upper limb exoskeleton and the kinematics and dynamics of the human arm. *Applied Bionics and Biomechanics*, 6(2):175–191, July 2009.

[44] Yuri Gloumakov, Adam Spiers, and Aaron Dollar. Adl human arm motion data, 2021.